


## Comparative study of classical theoretical descriptions of the ionization of atoms induced by few-cycle laser pulses

L. Sarkadi <sup>\*</sup>*Institute for Nuclear Research of the Hungarian Academy of Sciences (MTA Atomki), P.O. Box 51., H-4001 Debrecen, Hungary*

(Received 16 January 2021; revised 28 April 2021; accepted 28 April 2021; published 17 May 2021)

We have investigated the performance of classical models in the description of the single and double ionization of argon induced by 4-fs, 750-nm linearly polarized laser pulses by comparing the calculated quantities with existing experimental data, primarily the results of the systematic measurements of Kübel *et al.* [*Phys. Rev. A* **93**, 053422 (2016)], in the intensity range  $(1-10) \times 10^{14} \text{ Wcm}^{-2}$ . The comparison involved different one- and two-electron models based on the classical ensemble approximation. The analysis covered single- and double-ionization probabilities and their ratios, longitudinal momentum distributions of the  $\text{Ar}^+$  and  $\text{Ar}^{2+}$  recoiled ions, and the carrier-envelope-phase-dependent asymmetry of the yield of the  $\text{Ar}^+$  and  $\text{Ar}^{2+}$  ions.

DOI: [10.1103/PhysRevA.103.053113](https://doi.org/10.1103/PhysRevA.103.053113)

### I. INTRODUCTION

In the past two decades the development of laser technology has led to routine use of laser pulses as short as a few optical cycles for study of light-matter interactions. Particularly, the application of few-cycles pulses made it possible to explore the electron dynamics in the photoionization processes in unprecedented detail. Obviously, for such pulses the electron emission is practically confined to one optical cycle, which allows us to trace the process with sub-fs time resolution [1]. This property, besides its great fundamental importance, simplifies the theoretical treatment of the photoionization, particularly considering the double (multiple) electron emission. In a certain range of the laser intensity the latter dominantly proceeds via the rescattering mechanism: The first ionized electron in the next half optical cycle is driven back by the laser field, and collides with the parent ion inelastically, leading to emission of a further electron. For a long laser pulse multiple rescattering may occur, which impedes the theoretical interpretation of the experimental results. Using few-cycle laser pulses in an experiment, the contribution of the multiple rescattering can be excluded.

For a linearly polarized long laser pulse the contributions of the laser-matter interaction effects belonging to the opposite directions of the densely oscillating electric field are balanced. For photoionization this leads to symmetric electron emission. For a few-cycle pulse this is generally not the case; the emission is asymmetric [2]. The asymmetry depends on the phase of the carrier wave with respect to the pulse envelope, called carrier-envelope phase (CEP).

The first demonstration of production of intense, few-cycle laser pulses with a stable CEP [3] has initiated a wave of investigations to explore the CEP-dependent aspect of the photoionization [4–21,34,35] (for a review see, e.g., Refs. [22,23]). The measurement of the CEP-dependent quan-

ties represents a challenge, the experiments in this field are of great complexity. An important development in the experimental technique was the combination of the control of CEP with the cold target recoil ion momentum spectroscopy (COLTRIMS) [4]. Using the latter method, the momentum of all the reaction products can be determined (for a review see, e.g., Ref. [24]).

By means of COLTRIMS valuable information has been obtained about the role of the electron-electron correlation in the photoionization induced by few-cycles laser pulses [4,9,11,12,15–17]. These experiments mostly focused on the phenomenon of the nonsequential double ionization (NSDI, for a review see, e.g., Ref. [25]). NSDI proceeds via the rescattering mechanism discussed above. At lower laser intensities the probability of NSDI is higher by orders of magnitude than that expected assuming independent ionization of the two electrons [sequential double ionization (SDI)]. This is an unprecedented manifestation of the electron correlation in atomic physics, which explains the great interest towards NSDI.

The measurements differential with respect to CEP provided data for a stringent test of the performance and validity of the photoionization theories. A considerable amount of theoretical works, applying quantum mechanical, classical, and semiclassical models have been dealing with the CEP-dependent properties of the photoemission. The quantum mechanical approaches included the solution of the time-dependent Schrödinger equation [6–8,13,19], models using the strong-field approximation [5,14], and a two-step treatment of the recollision mechanism, called quantitative rescattering theory [10]. The classical models are based on the solution of the Newton's equation of motion [34,35,43], while in the semiclassical approaches the tunneling ionization step of the full process is treated quantum mechanically [5,6,11,12,17,18,26–28].

This work was motivated by the comprehensive experimental study of the multiple ionization of argon induced by CEP-tagged single-cycle linearly polarized infrared laser

<sup>\*</sup>sarkadil@atomki.hu

pulses carried out by Kübel *et al.* [17]. By performing kinematically complete measurements in a broad range of the laser intensity, the goal of the authors of this study was to provide benchmark data for a rigorous test of the theoretical models. They compared the obtained highly differential data with results of semiclassical calculations. The applied one-dimensional, single-active electron model is based on solution of coupled rate equations that govern the time evolution of the occupation probabilities of the Ar, Ar<sup>+</sup>, and Ar<sup>2+</sup> ground states, as well as the lowest excited Ar<sup>++</sup> state. The transition rates between the ionic states are determined by an extended version [29] of the Ammosov-Delone-Krainov (ADK) theory [30]. The authors considered only the excitation channel in the rescattering process, in which the scattering angle  $\beta$  was a free parameter of the model. A reasonable agreement between most of the experimental data and the model was achieved by multiplying the measured intensity by a factor of 2.5. This discrepancy was resolved by a comprehensive theoretical analysis of the measurements of Kübel *et al.* [17] carried out by Chen *et al.* [18] using a three-dimensional, two-active-electron semiclassical model. In this model the primary tunneling ionization was also treated by the ADK theory. The only approximation of the model was the choice of the initial phase-space coordinates of the two electrons following the tunneling.

Here we compare the systematic measuring data reported in Ref. [17] together with a few previously measured data [9,11] with the results of classical and semiclassical mechanical calculations that we carried out in different models in an intensity range  $(1-10) \times 10^{14} \text{ Wcm}^{-2}$ . The comparison involves quantities as single- and double-ionization probabilities, the longitudinal momentum distributions of the recoiled Ar<sup>+</sup> and Ar<sup>2+</sup> ions, and the asymmetry parameter accounting for the CEP effects.

## II. THEORY

For the classical description of the laser-induced ionization we used different versions of the classical ensemble approximation (CEA) model. CEA is based on the classical trajectory Monte Carlo (CTMC) method proposed originally by Abrines and Percival [31] for the description of ion-atom collisions. In the method the classical mechanical equations of motion of the particles are solved. We applied the three-dimensional, nonrelativistic, three-body version of the theory.

Due to the important role of the electron correlation effects in the regarded processes, reasonable results are expected from models that include the electron-electron interaction. In the classical treatment of the multielectron atom one is faced with the difficulty due to its instability. Classically the energy exchange between the electrons is not limited, after a time unphysical autoionization occurs: even in the absence of the external field the energy of one of the electrons becomes lower than the ground-state binding energy, while the other electron gains enough energy to be ionized. To prevent this, several methods have been proposed (for a review see, e.g., Ref. [32]). We made the calculations in two models in which the autoionization is prevented by suitably chosen atomic potentials, namely by a soft-Coulomb potential and by a Heisenberg-core potential. The former is referred to as CEA-SC. The latter

model is considered as a semiclassical one due to the strong quantum mechanical effect exerted by the Heisenberg potential throughout the time propagation, therefore it is called SCEA-H.

In the above models the electron correlation effects were expressed by considering two active electrons. For a comparison we made also calculations in an uncorrelated CEA model using the single-active-electron approximation. In the latter calculations single- and double-ionization probabilities were determined in the framework of the independent particle model (IPM), therefore we refer to this approach as CEA-IPM.

The quantum mechanical (QM) treatment of the regarded processes was beyond the scope of the present work, although a QM effect, namely the tunneling ionization was taken into account in the applied semiclassical model (referred as SCEA model). At the same time, it was interesting to compare the obtained results at least with the predictions of an uncorrelated QM theory. For this purpose we chose the ADK theory, and applied IPM to derive single- and double-ionization probabilities.

We note that in the reported simulations we did not include the focal volume averaging. However, we discuss its expected effect on the calculated quantities.

### A. CEA-SC model

In the model two  $3p$  electrons of the argon atom with total binding energy of  $-1.5946$  a.u. (sum of the first and second ionization energy) were chosen as active electrons orbiting around an atomic core of charge  $Z_{\text{core}} = 2$ . The atom is stabilized by replacing the Coulomb potential for the electron-core ( $e$ - $c$ ) and the electron-electron ( $e$ - $e$ ) interaction with a soft potential [33] defined as

$$V_{ij} = \frac{Z_i Z_j}{\sqrt{r_{ij}^2 + c_{\alpha\beta}^2}}. \quad (1)$$

Here  $Z_i$  and  $Z_j$  are the charges of the  $i$ th and  $j$ th particle, and  $r_{ij}$  is the distance between them. The  $c_{\alpha\beta}$  parameter is different for the  $e$ - $c$  and  $e$ - $e$  interaction. We note that the soft-core Coulomb potential has been widely applied in the theoretical works dealing with the laser-induced ionization of atoms [34–50]. For argon  $c_{ec} = 1.5$  and  $c_{ee} = 0.05$  have been proved to be the best values [34,35,41–43,45,46].

With the potential (1) the Newton's equations of motion for the three particles (the atomic core and the two electrons) of masses  $m_i$  interacting with the laser pulse

$$m_i \frac{d^2 \mathbf{r}_i}{dt^2} = \sum_{j(\neq i)=1}^3 -\nabla_{\mathbf{r}_i} [V_{ij}(r_{ij})] + Z_i \mathbf{E}(t) \quad (2)$$

take the following form:

$$m_i \frac{d^2 \mathbf{r}_i}{dt^2} = \sum_{j(\neq i)=1}^3 \frac{Z_i Z_j}{r'_{ij}{}^3} \mathbf{r}_{ij} + Z_i \mathbf{E}(t) \quad (3)$$

with

$$r'_{ij} = \sqrt{r_{ij}^2 + c_{\alpha\beta}^2}.$$

The laser pulse with wavelength of 750 nm was assumed to be of Gaussian shape with full width of half-maximum (FWHM) of 4 fs (intensity). Accordingly, the electric field  $\mathbf{E}(t)$  was taken as

$$\mathbf{E}(t) = E_0 \{\exp[-(t/\tau)^2]\}^{1/2} \cos(\omega t + \phi) \hat{\mathbf{k}}. \quad (4)$$

Here  $\omega$  is the frequency of the laser light,  $\tau$  is obtained from the relationship  $\text{FWHM} = 2\tau\sqrt{\ln 2}$ , and  $E_0$  is the amplitude of the electric field.  $E_0$  in atomic units is related to the laser intensity  $I$  expressed in W/cm<sup>2</sup> by  $E_0 = 0.533 \times 10^{-8} \sqrt{I}$ .  $\hat{\mathbf{k}}$  is a unit vector along the  $z$  axis defining the direction of the polarization. At the beginning and end of the pulse the electric field decreased to 0.3% of its maximum value.

### B. SCEA-H model

In SCEA-H the two active electrons of argon are considered in the same way as in the CEA-SC. The autoionization of the atom in this case is prevented by a Heisenberg-core potential proposed originally by Kirschbaum and Wilets [51] to stabilize the classically described multielectron atoms and molecules. This potential has been widely applied in investigations of atomic collisions [32] and laser-atom (-molecule) interactions [52–60]. Since it is a momentum-dependent potential, the time evolution of the system can be determined by the canonical equations:

$$\frac{d\mathbf{r}_i}{dt} = \frac{\partial H}{\partial \mathbf{p}_i}, \quad \frac{d\mathbf{p}_i}{dt} = -\frac{\partial H}{\partial \mathbf{r}_i}. \quad (5)$$

Here  $\mathbf{r}_i$  and  $\mathbf{p}_i$  are the position and momentum of the particles. The Hamiltonian  $H$  is expressed as

$$H = \sum_{i=1}^3 \frac{p_i^2}{2m_i} + \frac{1}{|\mathbf{r}_{1c} - \mathbf{r}_{2c}|} + \sum_{i=1,2} \left[ -\frac{2}{r_{ic}} + V_H(r_{ic}, p_{ic}) \right] - \sum_{i=1}^3 Z_i \mathbf{r}_i \mathbf{E}(t), \quad (6)$$

where  $\mathbf{r}_{ic}$  and  $\mathbf{p}_{ic}$  ( $i = 1, 2$ ) are the relative position and momentum of the two electrons with respect to the atomic core.  $V_H(r, p)$  is the Heisenberg-core potential:

$$V_H(r, p) = \frac{\xi^2}{4\alpha r^2} \exp\{\alpha[1 - (rp/\xi)^4]\}. \quad (7)$$

Following Refs. [57–59], we made our calculations with  $\alpha = 2$  and  $\xi = 1.225$ . An important property of this potential is that at a given value of  $\alpha$  the value of  $\xi$  can be chosen in a way that the minimum of the one-electron Hamiltonian agrees with the second ionization energy ( $-1.0154$  a.u. for argon). For the above parameter values the minimum energy is slightly smaller ( $-1.065$  a.u. [58]). The reason for the choice of the less optimal parameters is that at the exact energy match the two-electron orbits are prohibited energetically.

### C. CEA-IPM model

In this one-electron model the Newton's equations of motion (2) are solved for two particles moving in the electric field of the laser pulse: a single active electron chosen as a  $3p$  electron of argon and the atomic core. The core in this

case, unlike for CEA-SC and SCEA-H, interacts with the electron via a realistic screened Coulomb potential based on Hartree-Fock calculations [61]:

$$V(r) = -\{Z - (N_e - 1)[1 - \Omega(r, \eta, \zeta)]\}/r, \quad (8)$$

where  $Z$  is the nuclear charge,  $N_e$  is the number of the electrons in the atom (ion), and

$$\Omega(r, \eta, \zeta) = \{(\eta/\zeta)[\exp(\zeta r) - 1] + 1\}^{-1}.$$

$\eta$  and  $\zeta$  are parameters that depend on  $N_e$  and  $Z$ .

The Monte Carlo calculations solving the Newton's equations for a large number of laser-atom interaction events result in one-electron ionization probability  $p_i$  (the ratio of events leading to ionization to the total number of trials). For a multielectron atom the independent-particle model (IPM) can be applied to determine  $n$ -fold ionization probability  $P_n$ . For an atom having  $N$  electrons in the considered shell  $P_n$  is obtained by the following binomial expression:

$$P_n = \binom{N}{n} p_i^n (1 - p_i)^{(N-n)}. \quad (9)$$

In the present work we had to take into consideration the strong dependence of  $p_i$  on the binding energy of the electron in the investigated range of the laser intensity. After the ionization of the first electron the probability of the ionization of the second, the third, etc. electron is greatly reduced due to the increased  $n$ -fold ionization energies. Therefore, we used a more realistic form of the above expression. We took into account the dependence of  $p_i$  on the ionization energy, and in (9) we neglected the terms corresponding to higher than the second ionization energy. In this way the single-ionization probability, denoted by  $P_{si}$ , is expressed as

$$P_{si} = \binom{N}{1} p_i^{(1)} (1 - p_i^{(2)}). \quad (10)$$

The double-ionization probability, denoted by  $P_{di}$ , is given by

$$P_{di} = \binom{N}{2} p_i^{(1)} p_i^{(2)}. \quad (11)$$

In the above equations  $p_i^{(1)}$  and  $p_i^{(2)}$  are the one-electron ionization probabilities obtained by calculations carried out with the first and second ionization energy. In these calculations the parameters in Eq. (8) were as follows. For  $p_i^{(1)}$  (ionization of  $\text{Ar}^0$ )  $N_e = 18$ ,  $\eta = 3.50$ , and  $\zeta = 0.957$ . For  $p_i^{(2)}$  (ionization of  $\text{Ar}^+$ )  $N_e = 17$ ,  $\eta = 3.74$ , and  $\zeta = 1.17$ .

### D. ADK theory

We considered a modified version of the theory, which was proposed to extend its validity to laser intensities higher than the tunneling regime [29]. This was done by multiplying the tunneling ionization rate  $W_{\text{TI}}$  of the original theory [30] by an empirical factor:

$$W(F) = W_{\text{TI}}(F) \exp[-\alpha(Z_c^2/I_p)(F/\kappa^3)]. \quad (12)$$

Here  $F = |eE(t)|$  is the electric field strength,  $I_p$  is the ionization energy, and  $\kappa = \sqrt{2I_p}$ .  $\alpha$  and  $Z_c$  are parameters that depend on the atomic number and ionic state of the atom.

$W_{\text{TI}}(F)$  is expressed as

$$W_{\text{TI}}(F) = \frac{C_l^2}{2^{|m|}|m|!} \frac{(2l+1)(l+|m|)!}{2(l-|m|)!} \frac{1}{\kappa^{2Z_c/\kappa-1}} \times \left(\frac{2\kappa^3}{F}\right)^{2Z_c/\kappa-|m|-1} \exp(-2\kappa^3/3F), \quad (13)$$

where  $l$  and  $m$  are the angular momentum quantum numbers of the electron in the considered shell of the atom.  $C_l$  is a parameter of the theory determined by atomic structure calculations.

According to Ref. [29] one-electron ionization probability can be calculated as

$$p_i = 1 - \exp\left\{-\int_{-\infty}^{\infty} W[F(t)] dt\right\}. \quad (14)$$

In the ADK model we determined single- and double-ionization probabilities for argon in the same way, as for CEA-IPM, applying Eqs. (10) and (11). For this purpose we calculated the  $p_i^{(1)}$  and  $p_i^{(2)}$  probabilities for the first and second ionization energy using Eq. (14). In these calculations the parameters in Eqs. (12) and (13) were as follow. For  $\text{Ar}^0$ :  $C_l = 2.44$  [62],  $I_{p1} = 0.579$ ,  $Z_c = 1$ , and  $\alpha = 9$ . For  $\text{Ar}^+$ :  $C_l = 2.44$ ,  $I_{p2} = 1.0154$ ,  $Z_c = 2$ , and  $\alpha = 8$ . Only the  $3p$  electrons of argon were considered, the corresponding  $W(F)$  ionization rates were averaged over the magnetic quantum number  $m$ .

### E. SCEA model

In this hybrid quantum-classical two-electron model the first step of the ionization process is the tunneling of one of the electrons through the barrier formed by the atomic core potential and the electric potential of the laser pulse. To include the tunneling in the model, we followed the time development of the pulse from the beginning in small steps,  $\Delta t_i$ . At each step we calculated the probability of tunneling at time  $t_i$  using the modified ADK theory:  $\Delta p_i = 2W[F(t_i)]\Delta t_i$  (the factor 2 accounts for the two electrons). If  $\Delta p_i$  was smaller than  $\xi$  chosen randomly in the interval  $[0, 1]$ , then the next time step was considered. This procedure was continued until  $\Delta p_i > \xi$ , i.e., until the occurrence of tunneling. One can show that such a procedure alone (i.e., without the two-electron dynamics) leads to a total tunneling ionization probability  $p_i$  given by Eq. (14).

After tunneling the initial phase-space coordinates of the liberated electron and those of the remaining electron were calculated (see the next Sec. IIF), and the time propagation of the system was determined by solving the Newton's equations (2). Here we did not apply the  $Z_{\text{core}} = 2$  approximation for the electron-core interaction, but used the screened Coulomb potential expressed by Eq. (8).

### F. Choice of the initial phase-space electron coordinates

In CEA-SC and SCEA-H for the choice of the initial position and momentum coordinates of the electrons we applied a similar trial and error method as that proposed by Cohen [32]. In the first step of our procedure we treat the two electrons independently. We choose the magnitude of their position and momentum randomly in a given interval with uniform

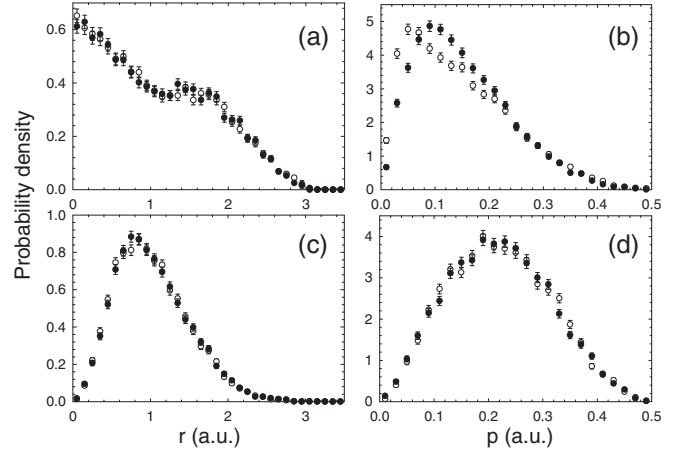


FIG. 1. One-electron initial position and momentum distributions in argon. (a) and (c) refer to the position before and after equilibration, respectively; (b) and (d) show the corresponding momentum distributions. The closed and open circles represent the method applied in the present work and that followed in Ref. [34], respectively.

distribution. To minimize the calculation time we optimized the length of the intervals. For CEA-SC we used the interval  $[0, 4.7$  a.u.] for the position, and  $[0, 1.7$  a.u.] for the momentum. For SCEA-H the corresponding intervals were  $[0, 3$  a.u.] and  $[0, 2$  a.u.]. We determine the angular coordinates of the electrons also randomly following the prescription the one-electron CTMC (see, e.g., Ref. [63]). Then we determine the total energy of the two electrons including their interaction. The sampling was accepted if the difference between the calculated energy and the binding energy of the two electrons was within 1%.

The equations of motion were solved using a fifth-order Runge-Kutta method. The integration of the equations was started well before the pulse to ensure the equilibration of the distribution of the phase space coordinates of the two electrons. The equilibrium was reached allowing the electrons to circulate around the nucleus 20 times. After the pulse in case of a double-ionization event the integration was continued until the energies of the electrons reached their asymptotical values.

We note that there is no unambiguous procedure for the determination of the initial position and momentum coordinates of the electrons. In the literature several different methods can be found. For example, in Ref. [34] first the classically allowed position coordinates for the total binding energy of the two electrons are determined, then the available kinetic energy is randomly distributed between the electrons in the momentum space. At the same time, one expects that as a result of the equilibration the different methods converge more or less to the same distributions of the phase space coordinates. This is illustrated in Fig. 1 where the results of calculations obtained by the present method and that used in Ref. [34] are compared. For the position the two methods lead to the same distributions both before and after the equilibration. For the momentum there is a difference between the two approaches initially, which, however, disappears after the equilibration.

For CEA-IPM we applied the well-established prescription the one-electron CTMC [63] for the determination of the phase-space electron coordinates in the case of non-Coulombic electron-core interaction.

For SCEA at the time moment  $t_0$  of the tunneling the exit coordinate of the electron  $z_0$  was obtained from the root  $\eta_0$  of the equation (in a.u.)

$$-\frac{1}{4\eta} - \frac{1}{8\eta^2} - \frac{F(t_0)\eta}{8} = -\frac{I_{p1}}{4} \quad (I_{p1} > 0) \quad (15)$$

as  $z_0 = -\text{sign}[eE(t_0)]\eta_0/2$ . The above equation was deduced from the form of the Schrödinger equation written for a hydrogenlike atom in a static outer electric field, and expressed in parabolic coordinates [64–66]. For  $F(t_0) > 0.149$  a.u.  $\eta_0$  is complex, which means an upper limit of  $7.8 \times 10^{14}$  Wcm $^{-2}$  laser intensity for the present SCEA calculations. We note that this limit means a restriction only in the below-the-barrier intensity regime, by a suitable choice of the initial conditions the application of SCEA can be extended for higher intensities [67].

The  $x$  and  $y$  component of the tunneled electron were chosen as  $x_0 = y_0 = 0$ . Its longitudinal velocity component  $v_{z0}$  was set to be zero, the transverse velocity  $v_{\perp}$  was chosen randomly according to the distribution  $\rho(v_{\perp}) = c v_{\perp} \omega(v_{\perp})$ . Here  $\omega(v_{\perp}) = \exp[-v_{\perp}^2 \kappa / F(t_0)]$  is the transverse velocity distribution derived by the adiabatic treatment of the tunneling ionization [68]. The normalization

$$\int_0^{2\pi} \int_0^{\infty} \rho(v_{\perp}) dv_{\perp} d\varphi = 1$$

results in  $c = \kappa / \pi F(t_0)$ . The  $v_x$  and  $v_y$  components were calculated as  $v_{x0} = v_{\perp} \cos \varphi$  and  $v_{y0} = v_{\perp} \sin \varphi$ , where  $\varphi$  was chosen randomly in the interval  $[0, 2\pi]$ .

The initial phase-space coordinates of the other electron bound with the second ionization energy in the atom were determined according to the microcanonical distribution [63] in the same way as for the CEA-IPM calculations.

### III. RESULTS AND DISCUSSION

#### A. Ionization probabilities

The results of the calculations obtained for the single- and double-ionization probabilities (averaged over CEP) are shown in Figs. 2 and 3 as a function of the laser intensity. For CEA-SC, SCEA-H, and SCEA the plotted probabilities are those obtained directly from the calculations, i.e., values that belong to electron emission from a two-electron model atom. For the one-electron CEA-IPM and ADK models the corresponding quantities were obtained by Eqs. (10) and (11) with  $N = 2$ . Although no experimental data exist for the ionization probability, the comparison of the predictions of the different models provides important information concerning their performance in the description of the ionization, particularly with respect to the modified ADK theory [29]. Since in the latter model the original ADK theory was corrected to reproduce the results obtained by the solution of the time-dependent one-electron Schrödinger equation, in this way as a quantum mechanical description it can be considered as a standard in the comparisons with other theories, at least for single ionization.

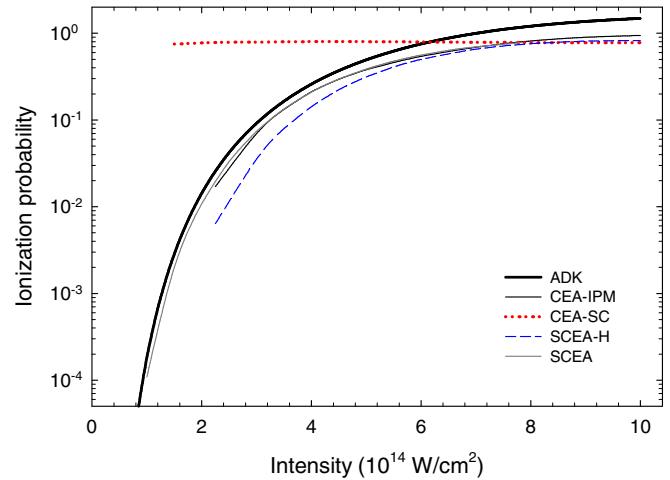


FIG. 2. Calculated single-ionization probabilities. The ADK, CEA-IPM, CEA-SC, SCEA-H, and SCEA models are represented by black thick, black thin, dotted red, dashed blue, and gray lines.

According to the figure, for the single ionization CEA-IPM, SCEA-H, and SCEA are in a reasonable agreement with ADK. The better agreement seen for CEA-IPM and SCEA can be explained by the more realistic screened electron-core potential applied in these models as compared to the  $Z_{\text{core}} = 2$  approximation in SCEA-H. CEA-SC completely fails to reproduce the strongly decreasing tendency of the ionization probability with decreasing laser intensity, it predicts almost a constant value.

For double ionization CEA-SC shows a decreasing tendency, but in the low-intensity range it overestimates ADK by many orders of magnitude. CEA-IPM, SCEA-H, and SCEA follow well the tendency of ADK, but strongly deviate from it in absolute value. SCEA-H shows a knee shape with an inflexion point around  $6 \times 10^{14}$  Wcm $^{-2}$ , indicating the increasing contribution of NSDI with decreasing intensity. SCEA also shows the knee shape, but in this case the inflexion point occurs at lower intensity, at around  $4 \times 10^{14}$  Wcm $^{-2}$ , and above this point the order-of-magnitude deviation from CEA-IPM suggests still a large contribution of NSDI. From the

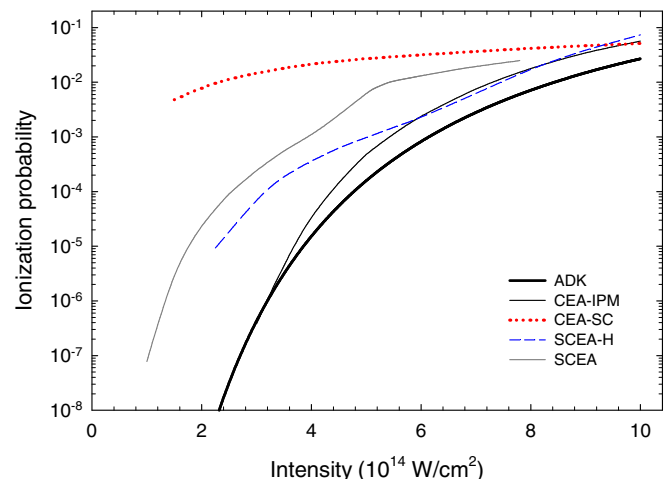


FIG. 3. The same as Fig. 2 but for double ionization.

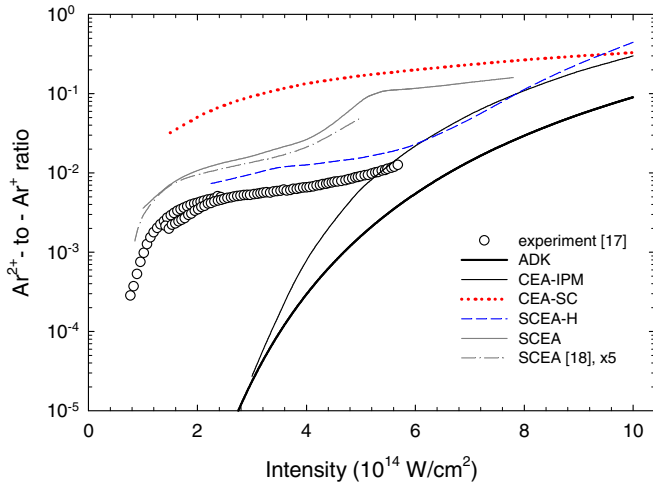


FIG. 4. Double-to-single ionization probability ratios. The circles denote the data measured by Kübel *et al.* [17]. The ADK, CEA-IPM, CEA-SC, SCEA-H, and SCEA models are represented by the black thick, black thin, dotted red, dashed blue, and gray line, respectively. The dashed-dotted gray line shows the semiclassical results of Chen *et al.* [18] after multiplication by a factor of 5.

difference between the results obtained by the two-electron models (CEA-H and SCEA) and the one-electron models (CEA-IPM and ADK) one may conclude that at the lowest considered laser intensity the probability of NSDI exceeds that of SDI by three orders of magnitude.

Figure 4 shows the double-to-single ionization probability ratios as a function of the laser intensity. In this case experimental data, namely the measured ratios of the yields of the  $\text{Ar}^{2+}$  and  $\text{Ar}^+$  ions [17] exist for the comparison with the predictions of the models. We note that for the CEA-SC, SCEA-H, and SCEA models the ratios for Ar were obtained from the primary probability ratios (i.e., the ratios of the probabilities in Figs. 2 and 3) by multiplying them by a factor of 5, considering that five times more electrons are available for the second ionization in the outer  $3p$  shell of Ar than for the two-electron atom. The same factor can be obtained in IPM by calculating the ratios of ratios using Eqs. (10) and (11) with  $N = 2$  for the two-electron atom and  $N = 6$  for Ar, respectively.

The experimental data show the characteristic knee shape. This structure is seen also for the SCEA-H and SCEA models, it is even more expressed here than in Fig. 3. All the other models fail to reproduce the structure. The SCEA-H results are higher than the measured data by almost a constant factor of about 1.8 along the overlapping intensity range of the theory and experiment. A similar intensity dependence is seen for SCEA below  $4 \times 10^{14} \text{ Wcm}^{-2}$ , but this model overestimates the data by a factor of about 3. With increasing intensity, however, the deviation between SCEA and experiment steeply increases. We note that Chen *et al.* [18] calculated this quantity applying the same semiclassical model as the present SCEA. Their results underestimated the measured ratios by a factor of 1.8, i.e., there is a discrepancy of factor of 5.4 between the two calculations. Assuming that the authors of Ref. [18] did not take into account the number of electrons available in the  $3p$  shell of Ar for the second ionization, we multiplied

their ratios by 5. According to Fig. 4, the corrected ratios agree well with the present SCEA results, the small difference between them is probably due to the  $Z_{\text{core}} = 2$  approximation applied in Ref. [18], as well as that in the latter work the ADK transition probability was calculated less realistically, using Eq. (20) of Ref. [68] (only with  $m = 0$ ) instead of using Eqs. (12) and (13) of the extended ADK theory. We note a further computational difference between the two calculations, namely that in Ref. [18] regularized coordinates [69] were employed for the treatment of the Coulomb singularity to provide a faster and more stable numerical time propagation.

Chen *et al.* [18] presented also SCEA results in which the focal volume effect on the double-to-single ionization probability ratio has been taken into account. In the present work we did not consider this effect, primarily because no detailed data have been published for the focusing geometry of the laser beams used in the experiment. However, we could estimate the focal volume effect from the SCEA results obtained by Chen *et al.* with and without including the effect. In the intensity range  $(1.4\text{--}3) \times 10^{14} \text{ Wcm}^{-2}$  the effect resulted in a decrease of the ratios at an average by a factor of 1.7. Considering the very similar intensity dependence of SCEA and SCEA-H, for the latter we may apply the same correction factor. This leads to an agreement between SCEA-H and the experiment within 10%. As a result of the correction, the present SCEA still overestimates the measured data by a factor of 1.8. At the same time, above  $4 \times 10^{14} \text{ Wcm}^{-2}$  the increasing volume effect (see Fig. 1 in Ref. [18]) compensates the steep increase found in the SCEA results, therefore its inclusion into the model expectedly results in an improvement in the description of the observed shape of the intensity dependence. The order-of-magnitude discrepancy between CEA-SC and the measured data, however, still remains after the focal volume correction.

## B. Recoil ion momentum distributions

For the ionization induced by a linearly polarized laser pulse one can estimate the maximum momentum transferred to the electron by the electric field along the direction of the polarization vector by neglecting the interaction of the ionized electron with the Coulomb field of the atom. A simple calculation results in  $2\sqrt{U_p}$  (in atomic units), where  $U_p$  is the ponderomotive energy [25]. Accordingly, the spread of the longitudinal momentum distribution of the singly charged recoil ions produced in the photoionization is approximately limited by the values  $\pm 2\sqrt{U_p}$  [44]. For doubly charged ions the corresponding limits are  $\pm 4\sqrt{U_p}$ . This means that the measured longitudinal recoil ion momentum distribution strongly depends on the laser intensity, and thereby its measurement represents a sensitive test of the theory. Kübel *et al.* [17] in analyzing their experimental data determined the momentum distributions of the  $\text{Ar}^+$  and  $\text{Ar}^{2+}$  ions applying the semiclassical model mentioned in Sec. I. They obtained good agreement with the measured distributions only when the experimental intensities were multiplied by 2.5.

In Fig. 5 the (CEP-averaged) results of the present calculations are compared with the measured longitudinal momentum distribution for the  $\text{Ar}^+$  ions at a selected laser

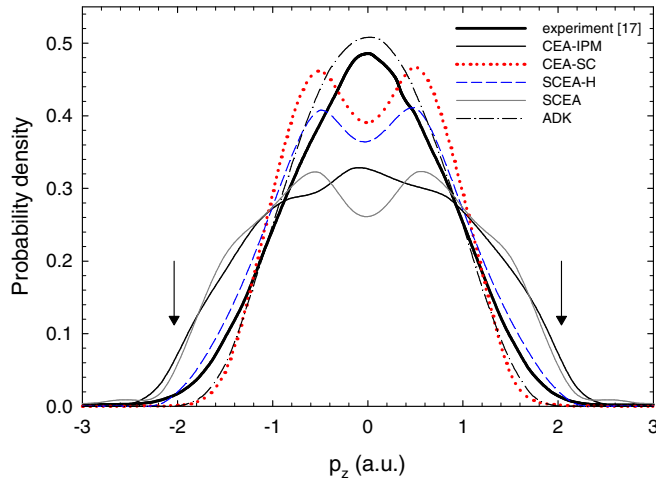


FIG. 5. The longitudinal momentum distribution for the  $\text{Ar}^+$  ions at laser intensity of  $5.4 \times 10^{14} \text{ Wcm}^{-2}$ . The black thick line denotes the measured distribution [17]. The CEA-IPM, CEA-SC, SCEA-H, and SCEA models are represented by the black thin, dotted red, dashed blue, and gray solid line, respectively. The dashed-dotted black line shows the ADK results. The arrows indicate the approximate theoretical maximum longitudinal momenta,  $\pm 2\sqrt{U_p}$ .

intensity of  $5.4 \times 10^{14} \text{ Wcm}^{-2}$  (the original experimental intensity). Each distribution is normalized to unit area. The momentum spread observed in the experiment is well reproduced by the present models, i.e., our calculations do not support the finding of Kübel *et al.* that the measured distribution belongs to a significantly increased laser intensity. At the same time, large differences can be observed between the predictions of the models. CEA-IPM and SCEA largely overestimate the width of the measured distribution. CEA-SC and particularly SCEA-H provide a reasonable description for momenta  $|p_z| > 1$ , but both models show a peak inversion around  $p_z = 0$ , in disagreement with the experiment. Peak inversion was found also for SCEA. The best agreement with the measured data is seen for ADK.

We note that ADK, in the form as it is expressed by Eqs. (12)–(14), is suitable only for calculation of transition rates and probabilities, not for momentum distributions. For the latter purpose we carried out a Monte Carlo simulation in which the probability of the tunneling ionization at a time moment  $t_i$  was determined by Eqs. (12)–(13), and the longitudinal momentum of the liberated electron at the end of the pulse ( $t_f$ ) was obtained using the strong-field approximation (SFA), i.e., neglecting the interaction between the electron and atomic core:

$$p_z(t_f) = p_z(t_i) + \int_{t_i}^{t_f} eE(t) dt. \quad (16)$$

Here the electric field  $E(t)$  is given by Eq. (4). We note that using  $\cos^2$ -shaped envelope function in (4) instead of Gaussian, the above integral is analytic, and leads practically to the same result as the Gaussian envelope. Equation (16) was solved with the widely applied approximation,  $p_z(t_i) = 0$ . We searched for the reason of the unexpected peak inversion found for CEA-SC, SCEA-H, and SCEA. It turned out that it is a few-cycle property of the classical descriptions: With

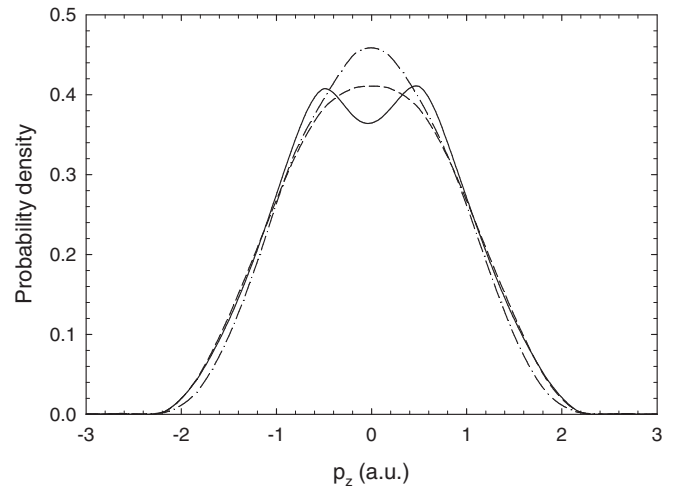


FIG. 6. The longitudinal momentum distribution for the  $\text{Ar}^+$  ions calculated in the SCEA-H model with pulse duration of 4 fs (solid line), 20 fs (dashed line), and 40 fs (dashed-dotted line) at laser intensity of  $5.4 \times 10^{14} \text{ Wcm}^{-2}$ .

increasing pulse duration the shape of the peak inversion disappears, the distribution approaches that obtained by ADK. This is demonstrated in Fig. 6, which shows the results of SEA-H calculations made with pulse durations of 4, 20, and 40 fs.

The spread of the longitudinal momentum distribution of the  $\text{Ar}^{2+}$  ions obtained in all our models is also in accordance with the experiment as well as the general theoretical expectation (see Fig. 7), i.e., our results confirm the correctness of the experimental laser intensity also in this case. As far as the performance of the models is concerned, an excellent agreement with the measured distribution is obtained by CEA-IPM and SCEA. SCEA-H also provided a reasonable description

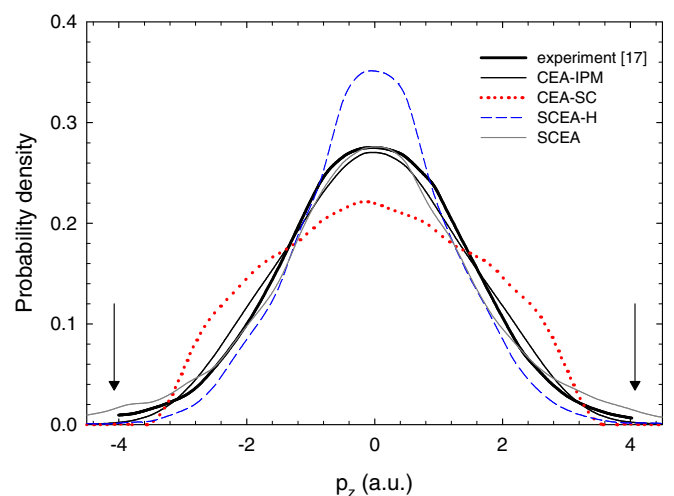


FIG. 7. The longitudinal momentum distribution for the  $\text{Ar}^{2+}$  ions at laser intensity of  $5.4 \times 10^{14} \text{ Wcm}^{-2}$ . The black thick line denotes the measured distribution [17]. The CEA-IPM, CEA-SC, SCEA-H, and SCEA models are represented by the black thin, dotted red, dashed blue, and gray line, respectively. The arrows indicate the approximate theoretical maximum longitudinal momenta,  $\pm 4\sqrt{U_p}$ .

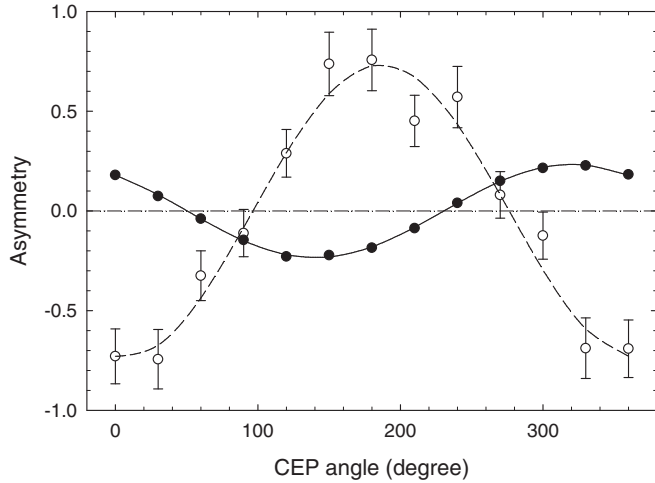


FIG. 8. CEP dependence of the asymmetry parameter obtained by the SCEA-H model for the single (closed circles) and double (open circles) ionization at laser intensity of  $2.25 \times 10^{14} \text{ Wcm}^{-2}$ . The lines are fits of the function (18) to the calculated values.

for  $|p_z| > 1$ , but it predicts too narrow distribution at smaller momentum values. CEA-SC completely fails to reproduce the measured distribution.

The way of calculation of the momentum of the  $\text{Ar}^{2+}$  ions in CEA-IPM needs some explanation. In this model two separate series of calculations are made using the first and second ionization energy. In the evaluation of the obtained results pairs of ionization events belonging to the two ionization energies are created randomly. From the momenta of the ionized electrons the momentum of the  $\text{Ar}^{2+}$  ions is determined using the momentum conservation law.

### C. CEP-dependent asymmetry

The asymmetry arising in the ionization of atoms induced by linearly polarized few-cycle laser pulses is characterized by the asymmetry parameter. At laser intensity  $I$  and CEP angle  $\phi$  it is defined as

$$A(I, \phi) = \frac{N_+(I, \phi) - N_-(I, \phi)}{N_+(I, \phi) + N_-(I, \phi)}. \quad (17)$$

Here  $N_+(I, \phi)$  and  $N_-(I, \phi)$  are the number of the ions recoiled with positive and negative momentum along the laser polarization, respectively. The dependence of  $A(I, \phi)$  on  $\phi$  is a sinusoidal function:

$$A(I, \phi) = A_0(I) \sin[\phi + \phi_0(I)]. \quad (18)$$

This function is fitted to the measured and calculated asymmetry parameters, and the obtained  $A_0(I)$  amplitudes and  $\phi_0(I)$  phases are used for the comparison between the experiment and theory. An example of the fitting made for the results of SCEA-H calculations at laser intensity of  $2.25 \times 10^{14} \text{ Wcm}^{-2}$  is shown in Fig. 8.

In Fig. 9 we compare the  $A_0(I)$  amplitudes for the yield of the  $\text{Ar}^+$  ion obtained by the considered models with results of experiments. SCEA-H and CEA-IPM correctly reproduce the slightly increasing tendency of  $A_0(I)$  with decreasing laser intensity seen in the measured data of Kübel *et al.* [17],

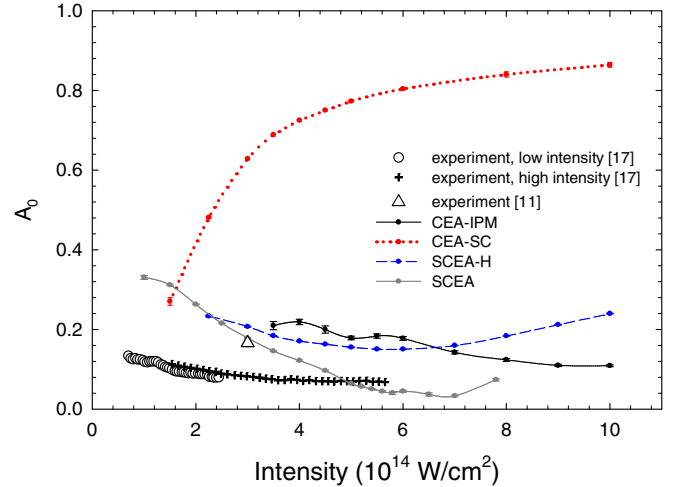


FIG. 9. The  $A_0(I)$  amplitude deduced from the CEP-dependent yield of the  $\text{Ar}^+$  ion according Eqs. (17)–(18). The circles and crosses denote the low- and high-intensity data measured by Kübel *et al.* [17], respectively. The triangle is an experimental result obtained by Bergues *et al.* [11]. The black, the dotted red, the dashed blue, and the gray line represent the CEA-IPM, CEA-SC, SCEA-H, and SCEA models, respectively.

although they overestimate the latter data by a factor of 2–3. SCEA predicts a similar, but stronger intensity dependence, approaching the measured data at larger intensities. At lower intensities, the value measured by Bergues *et al.* [11] at  $3 \times 10^{14} \text{ Wcm}^{-2}$  agrees well with SCEA, and supports also SCEA-H and CEA-IPM. CEA-SC is in complete disagreement with the experiments.

Figure 10 shows a comparison for the  $\text{Ar}^{2+}$  ion. Here only SCEA-H and SCEA agree at least qualitatively with the experiments: The  $A_0$  amplitude predicted by these models steeply increases with decreasing intensity in accordance with the observation by Kübel *et al.* [17]. SCEA-H shows a minimum at  $4.5 \times 10^{14} \text{ Wcm}^{-2}$ . It seems that the measured data also have

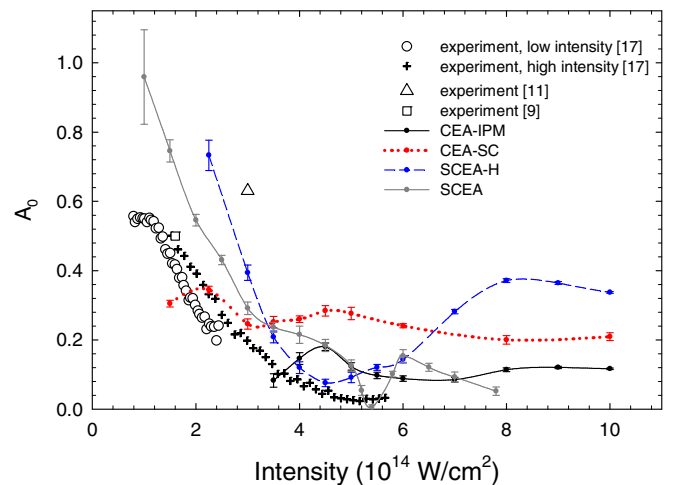


FIG. 10. The same as Fig. 9, but for the  $\text{Ar}^{2+}$  ion. Note a further experimental value ( $A_0 = 0.5$ ) shown by a square at  $I = 1.6 \times 10^{14} \text{ Wcm}^{-2}$ , measured by Johnson *et al.* [9].



a minimum at somewhat higher intensity. At this intensity SCEA also predicts a very narrow, resonancelike minimum. This feature is not seen in the experiment; in this intensity range SCEA-H provides a better qualitative description of the measured data than SCEA. In the low-intensity range both SCEA-H and SCEA overestimate the experiment by a factor of up to two. However, there are deviations of similar magnitude between the different experiments: The value measured by Bergues *et al.* [11] at  $3 \times 10^{14} \text{ Wcm}^{-2}$  is three times higher than that obtained by Kübel *et al.* At the same time, the  $A_0$  value measured by Johnson *et al.* [9] at  $1.6 \times 10^{14} \text{ Wcm}^{-2}$  agrees well with the measurements of Kübel *et al.*

We note that the SCEA calculations of Chen *et al.* [18] resulted in also a large asymmetry parameter at small intensities, however, their model predicts a less steep decrease of  $A_0(I)$  with decreasing intensity than the present SCEA model: The value presented by the authors at the highest considered intensity ( $5 \times 10^{14} \text{ Wcm}^{-2}$ ) is larger by a factor of 2.7 than that obtained in the present work. This large difference between the predictions of the two models is surprising, considering the good agreement found for the double-to-single ionization probability ratio. As we pointed out in Sec. III A, there are some differences between the ingredients of the two models. The effects due to the differences may be canceled or washed out for CEP-averaged relative quantities. For CEP-dependent quantities, however, the differences between the models may be strongly manifested.

We call attention to the increasing deviation between CEA-IPM and SCEA-H with increasing laser intensity for both the  $\text{Ar}^+$  and  $\text{Ar}^{2+}$  ion. This is an unexpected result, considering that the single- and double-ionization probabilities, as well as the  $\text{Ar}^{2+}$ -to- $\text{Ar}^+$  yield ratios predicted by the two models converge to each other with increasing intensity (see Figs. 2, 3, and 4). SCEA-H differs from CEA-IPM mostly in that the former includes the electron-electron interaction. The latter, however, has a small effect on the ionization process at high intensities. This means that the difference between the two models in description of the CEP-dependent asymmetry can probably be attributed to the different potentials applied for the electron-core interaction: a realistic screened Coulomb potential in CEA-IPM, and Coulomb potential with  $Z_{\text{core}} = 2$  together with the Heisenberg-core potential in SCEA-H. This observed sensitivity on the atomic potential has great significance: By measurement of the CEP-dependent asymmetry parameters of an atomic system using few-cycle laser pulses one may obtain valuable information about the potential.

Since in the experiments the CEP is only determined up to an unknown offset value, we could not compare the calculated  $\phi_0(I)$  values with the corresponding measured quantities unambiguously. Instead, we considered the well-defined  $\text{Ar}^{2+}$ -to- $\text{Ar}^+$  relative phase,  $\Delta\phi_0(I) = \phi_0(I, \text{Ar}^{2+}) - \phi_0(I, \text{Ar}^+)$ . The calculated and measured  $\Delta\phi_0(I)$  values are plotted in Fig. 11. Here again SCEA-H and SCEA provide a reasonable description of the measured data, although the experiment does not show the abrupt increase of the calculated values at  $4 \times 10^{14} \text{ Wcm}^{-2}$ . Above this intensity both models predict a resonancelike dependence of the relative phase but with largely differing widths.

For the CEP-dependent asymmetry the focal volume effect can be estimated also from the SCEA calculations of

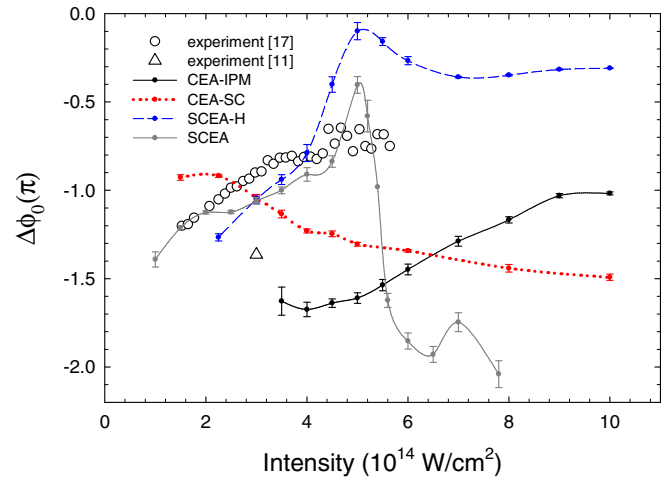


FIG. 11. The relative phase between the CEP dependence of the  $\text{Ar}^{2+}$  and  $\text{Ar}^+$  ion yield. The circles denote the data measured by Kübel *et al.* [17]. The triangle shows the experimental result of Bergues *et al.* [11]. The black, the dotted red, the dashed blue, and the gray line represent the CEA-IPM, CEA-SC, SCEA-H, and SCEA models, respectively.

Chen *et al.* [18]. For the double ionization in the intensity range  $(1-5) \times 10^{14} \text{ Wcm}^{-2}$  the inclusion of the effect into the model resulted in an increase of the  $A_0(I)$  amplitude by a factor up to 1.5. This means that the consideration of the focal volume effect would only slightly change the performance of the present models in the description of the measured data shown in Fig. 10. Particularly, the predictions of SCEA-H and SCEA would deviate more from the data of Ref. [17], while they would support better the value measured in Ref. [11].

From the work in Ref. [18] information concerning the focal volume effect can be obtained also for  $\phi_0(I)$  in case of double ionization. However, we cannot use this information, because in those calculations the absolute phase was considered, while our analysis is based on the calculation of the relative phase between the double and single ionization.

Finally we note that the details of the correlated two-electron emission induced by few-cycle laser pulses have been investigated in several works [11,12,18,34,35,43] by tracing the classically calculated electron trajectories. Such an analysis was beyond the scope of the present work. To get an idea about the possible double-ionization mechanisms in this model, we followed the time evolution of the two-electron trajectories of several randomly chosen ionization events at laser intensity of  $3 \times 10^{14} \text{ Wcm}^{-2}$ . We found examples for both the recollision-impact-ionization (RII) and the recollision-induced-excitation-with-subsequent ionization (RESI) (see Figs. 12 and 13). For RESI the second ionization step was delayed with respect to the first one dominantly by half optical cycle; in a few cases the delay was one optical cycle. According to the figures, in the first ionization step the electron driven back by the field towards the atom is not completely free, rather it is in a highly excited Rydberg state. On its way back to the atom its energy is mostly a small negative value, and it does not move very far away from the atom. This picture of rescattering generally holds for

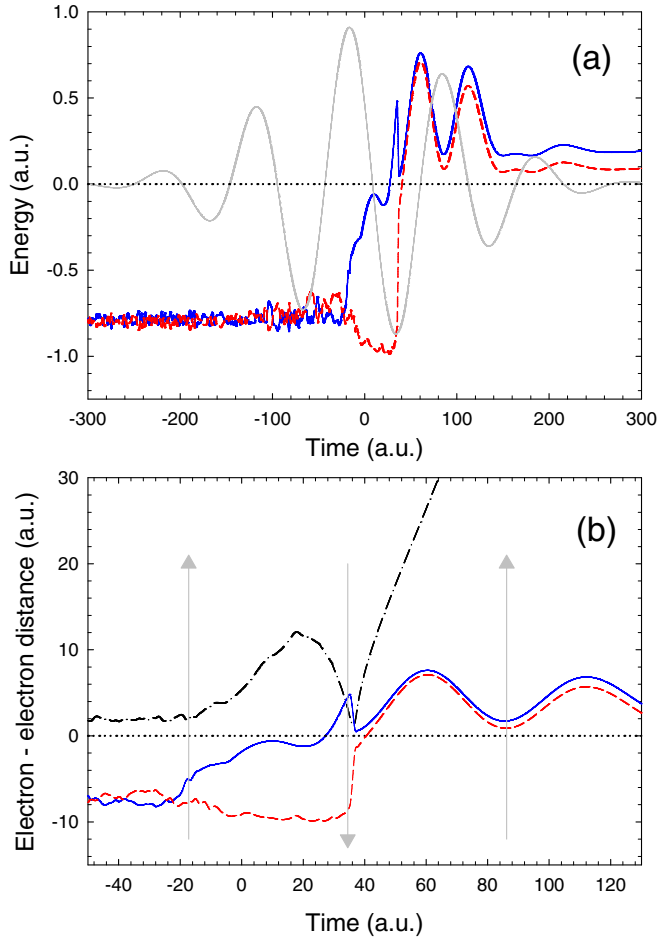


FIG. 12. A double-ionization event proceeding through the recollision-impact-ionization (RII) mechanism obtained in the SCEA-H model at laser intensity of  $3 \times 10^{14} \text{ Wcm}^{-2}$ . In (a) the blue and the dashed red line denote the one-electron energies, the gray line denotes the electric force of the laser light in arbitrary units. (b) shows the same event zooming into a shorter time interval. Here the dashed-dotted black line denotes the electron-electron distance, the electron energies are plotted in arbitrary units. The gray arrows show the positions of the positive and negative maxima of the electric force.

all double-ionization events, and it is more correct to call it quasiscattering.

#### IV. CONCLUSIONS

We have investigated the performance of classical models in the description of the single and double ionization of argon induced by few-cycle laser pulses by comparing the calculated quantities with existing experimental data in a broad range of the laser intensity. The main tendencies of the measured quantities, particularly the double-to-single ionization probability ratios and the amplitudes of the CEP-dependent asymmetry of the yield of the  $\text{Ar}^+$  and  $\text{Ar}^{2+}$  ions were well reproduced by the model using the Heisenberg-core potential for the stabilization of the two-electron atom (SCEA-H), as well as by the semiclassical model based on the ADK theory (SCEA). The orders-of-magnitude deviations found between

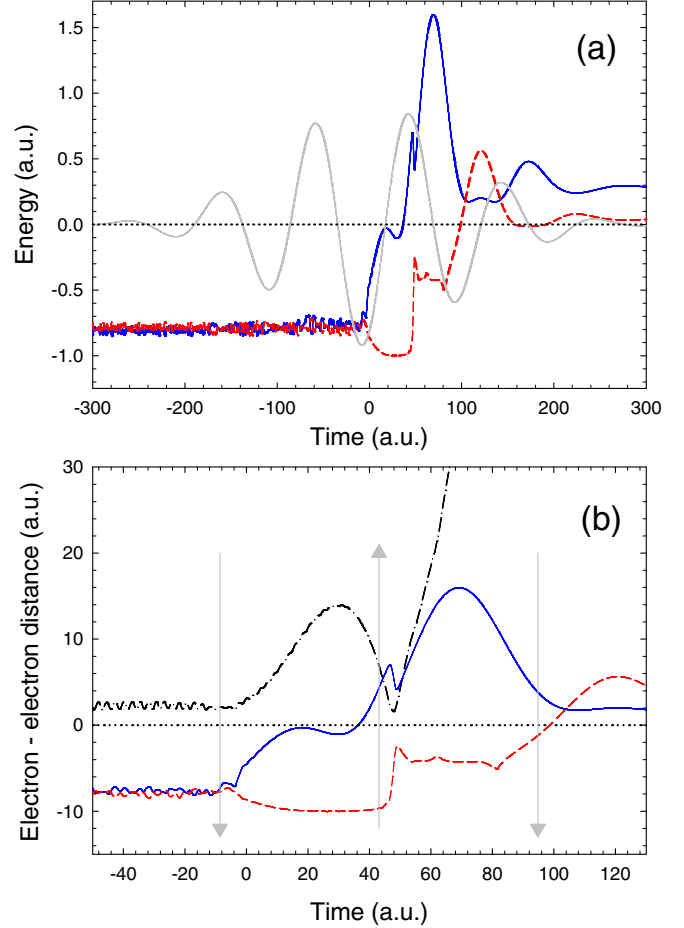


FIG. 13. The same as Fig. 12 but for a double-ionization event proceeding through the recollision-induced-excitation-with-subsequent ionization (RESI) mechanism.

the predictions of the different models for the ionization probabilities demonstrated the importance of these quantities in the assessment of the models. To draw firm conclusions from such a comparison the measurement of the ionization probabilities, i.e., the number of the ionization events per pulse shot and per atom would be highly desirable.

Our analysis made for the CEP-dependent asymmetry of the yield of the  $\text{Ar}^+$  and  $\text{Ar}^{2+}$  ions revealed an unexpected large sensitivity on the atomic potential applied in the models at high laser intensities. From this point of view valuable information is expected from the extension of the systematic experiments to laser intensities up to  $10^{15} \text{ Wcm}^{-2}$ .

Finally we note that in the present calculations we did not include the focal volume effect, primarily because no detailed data are available for the focusing properties of the laser beams used in the experiments. Furthermore, such calculations would need much computational efforts, particularly considering the spatial dependence of CEP, which is more complex for a focused few-cycle pulse than for a monochromatic beam [21]. However, we could estimate the focal volume effect from the results of the semiclassical calculations made by Chen *et al.* [18] with and without taking

into account the effect. From this point of view we analyzed the double-to-single ionization probability ratio, and the CEP-dependent asymmetry parameter for the double ionization. We found that the performance of the considered models for these quantities would not change drastically by the focal-volume averaging.

## ACKNOWLEDGMENTS

This work was supported by the Hungarian Scientific Research Fund (Grant No. K128621), the National Research, Development and Innovation Office (Grant No. 2018-1.2.1-NKP-2018-00010), and the National Information Infrastructure Development Program.

- [1] M. Hentschel, R. Kienberger, Ch. Spielmann, G. A. Reider, N. Milosevic, T. Brabec, P. Corkum, U. Heinzmann, M. Drescher, and F. Krausz, *Nature (London)* **414**, 509 (2001).
- [2] G. G. Paulus, F. Grasbon, H. Walther, P. Villorosi, M. Nisoli, S. Stagira, E. Priori, and S. De Silvestri, *Nature (London)* **414**, 182 (2001).
- [3] A. Baltuška, Th. Udem, M. Uiberacker, M. Hentschel, E. Goulielmakis, Ch. Gohle, R. Holzwarth, V. S. Yakovlev, A. Scrinzi, T. W. Hänsch, and F. Krausz, *Nature (London)* **421**, 611 (2003).
- [4] X. Liu, H. Rottke, E. Eremina, W. Sandner, E. Goulielmakis, K. O. Keeffe, M. Lezius, F. Krausz, F. Lindner, M. G. Schätzel, G. G. Paulus, and H. Walther, *Phys. Rev. Lett.* **93**, 263001 (2004).
- [5] C. Figueira de Morisson Faria, X. Liu, A. Sanpera, and M. Lewenstein, *Phys. Rev. A* **70**, 043406 (2004).
- [6] D. G. Arbó, E. Persson, K. I. Dimitriou, and J. Burgdörfer, *Nucl. Instrum. Methods Phys. Res., Sect. B* **267**, 330 (2009).
- [7] B. Eckhardt, J. S. Prauzner-Bechcicki, K. Sacha, and J. Zakrzewski, *Chem. Phys.* **370**, 168 (2010).
- [8] A. N. Grum-Grzhimailo, B. Abeln, K. Bartschat, D. Weffen, and T. Urness, *Phys. Rev. A* **81**, 043408 (2010).
- [9] N. G. Johnson, O. Herrwerth, A. Wirth, S. De, I. Ben-Itzhak, M. Lezius, B. Bergues, M. F. Kling, A. Senftleben, C. D. Schröter, R. Moshhammer, J. Ullrich, K. J. Betsch, R. R. Jones, A. M. Saylor, T. Rathje, K. Rühle, W. Müller, and G. G. Paulus, *Phys. Rev. A* **83**, 013412 (2011).
- [10] Zh. Chen, Y. Liang, D. H. Madison, and C. D. Lin, *Phys. Rev. A* **84**, 023414 (2011).
- [11] B. Bergues *et al.*, *Nature Commun.* **3**, 813 (2012).
- [12] N. Camus, B. Fischer, M. Kremer, V. Sharma, A. Rudenko, B. Bergues, M. Kübel, N. G. Johnson, M. F. Kling, T. Pfeifer, J. Ullrich, and R. Moshhammer, *Phys. Rev. Lett.* **108**, 073003 (2012).
- [13] J. M. N. Djiokap, S. X. Hu, W.-Ch. Jiang, L.-Y. Peng, and A. F. Starace, *New J. Phys.* **14**, 095010 (2012).
- [14] C. Figueira de Morisson Faria, T. Shaaran, and M. T. Nygren, *Phys. Rev. A* **86**, 053405 (2012).
- [15] M. Kübel, N. G. Kling, K. J. Betsch, N. Camus, A. Kaldun, U. Kleineberg, I. Ben-Itzhak, R. R. Jones, G. G. Paulus, T. Pfeifer, J. Ullrich, R. Moshhammer, M. F. Kling, and B. Bergues, *Phys. Rev. A* **88**, 023418 (2013).
- [16] M. Kübel, K. J. Betsch, N. G. Kling, A. S. Alnaser, J. Schmidt, U. Kleineberg, Y. Deng, I. Ben-Itzhak, G. G. Paulus, T. Pfeifer, J. Ullrich, R. Moshhammer, M. F. Kling, and B. Bergues, *New J. Phys.* **16**, 033008 (2014).
- [17] M. Kübel, C. Burger, N. G. Kling, T. Pischke, L. Beaufore, I. Ben-Itzhak, G. G. Paulus, J. Ullrich, T. Pfeifer, R. Moshhammer, M. F. Kling, and B. Bergues, *Phys. Rev. A* **93**, 053422 (2016).
- [18] A. Chen, M. Kübel, B. Bergues, M. F. Kling, and A. Emmanouilidou, *Sci. Rep.* **7**, 7488 (2017).
- [19] M. Kübel, M. Arbeiter, C. Burger, N. G. Kling, T. Pischke, R. Moshhammer, T. Fennel, M. F. Kling, and B. Bergues, *J. Phys. B* **51**, 134007 (2018).
- [20] D. Zille, D. Adolph, M. Möller, A. M. Saylor, and G. G. Paulus, *New J. Phys.* **20**, 063018 (2018).
- [21] Y. Zhang, D. Zille, D. Hoff, Ph. Wustelt, D. Würzler, M. Möller, A. M. Saylor, and G. G. Paulus, *Phys. Rev. Lett.* **124**, 133202 (2020).
- [22] D. B. Milošević, G. G. Paulus, D. Bauer, and W. Becker, *J. Phys. B* **39**, R203 (2006).
- [23] B. Bergues, M. Kübel, N. G. Kling, C. Burger, and M. F. Kling, *J. Sel. Top. Quantum Electron.* **21**, 8701009 (2015).
- [24] J. Ullrich, R. Moshhammer, A. Dorn, R. Dörner, L. Ph. Schmidt, and H. Schmidt-Böcking, *Rep. Prog. Phys.* **66**, 1463 (2003).
- [25] W. Becker, X. J. Liu, P. J. Ho, and J. H. Eberly, *Rev. Mod. Phys.* **84**, 1011 (2012).
- [26] A. Emmanouilidou, *Phys. Rev. A* **78**, 023411 (2008).
- [27] H. Price, A. Staudte, and A. Emmanouilidou, *New J. Phys.* **13**, 093006 (2011).
- [28] G. P. Katsoulis, A. Hadjipittas, B. Bergues, M. F. Kling, and A. Emmanouilidou, *Phys. Rev. Lett.* **121**, 263203 (2018).
- [29] X. M. Tong and C. D. Lin, *J. Phys. B* **38**, 2593 (2005).
- [30] M. V. Ammosov, N. B. Delone, and V. P. Krainov, *Sov. Phys. JETP* **64**, 1191 (1986).
- [31] R. Abrines and I. C. Percival, *Proc. Phys. Soc. London* **88**, 861 (1966).
- [32] J. S. Cohen, *Phys. Rev. A* **54**, 573 (1996).
- [33] Q. Su and J. H. Eberly, *Phys. Rev. A* **44**, 5997 (1991).
- [34] C. Huang, Y. Zhou, Q. Zhang, and P. Lu, *Opt. Express* **21**, 11382 (2013).
- [35] Y. Chen, Y. Zhou, Y. Li, M. Li, P. Lan, and P. Lu, *J. Chem. Phys.* **144**, 024304 (2016).
- [36] Th. Brabec, M. Yu. Ivanov, and P. B. Corkum, *Phys. Rev. A* **54**, R2551 (1996).
- [37] R. Panfili, J. Eberly, and S. Haan, *Opt. Express* **8**, 431 (2001).
- [38] R. Panfili, S. L. Haan, and J. H. Eberly, *Phys. Rev. Lett.* **89**, 113001 (2002).
- [39] P. J. Ho, R. Panfili, S. L. Haan, and J. H. Eberly, *Phys. Rev. Lett.* **94**, 093002 (2005).
- [40] Y. Zhou, Q. Liao, and P. Lu, *Phys. Rev. A* **82**, 053402 (2010).
- [41] Z. Zhang, J. Zhang, L. Bai, and X. Wang, *Opt. Express* **23**, 7044 (2015).
- [42] T. Wang, X. L. Ge, J. Guo, and X. S. Liu, *Phys. Rev. A* **90**, 033420 (2014).
- [43] F. Feng and L. Bai, *Chin. Opt. Lett.* **16**, 063201 (2018).
- [44] S. L. Haan, J. S. Van Dyke, and Z. S. Smith, *Phys. Rev. Lett.* **101**, 113001 (2008).

- [45] Q. Liao, A. H. Winney, S. K. Lee, Y. F. Lin, P. Adhikari, and W. Li, *Phys. Rev. A* **96**, 023401 (2017).
- [46] X. Wang and J. H. Eberly, *J. Chem. Phys.* **137**, 22A542 (2012).
- [47] L. Sarkadi, *J. Phys. B* **53**, 165401 (2020).
- [48] J. B. Watson, A. Sanpera, D. G. Lappas, P. L. Knight, and K. Burnett, *Phys. Rev. Lett.* **78**, 1884 (1997).
- [49] W.-C. Liu, J. H. Eberly, and S. L. Haan, and R. Grobe, *Phys. Rev. Lett.* **83**, 520 (1999).
- [50] Q. Liao and P. Lu, *Phys. Rev. A* **82**, 021403(R) (2010).
- [51] C. L. Kirschbaum and L. Wilets, *Phys. Rev. A* **21**, 834 (1980).
- [52] D. A. Wasson and S. E. Koonin, *Phys. Rev. A* **39**, 5676 (1989).
- [53] K. J. LaGattuta and J. S. Cohen, *J. Phys. B* **31**, 5281 (1998).
- [54] K. J. LaGattuta, *Eur. Phys. J. D* **2**, 267 (1998).
- [55] K. J. LaGattuta, *J. Phys. B* **33**, 2489 (2000).
- [56] P. B. Lerner, K. J. LaGattuta, and J. S. Cohen, *Phys. Rev. A* **49**, R12 (1994).
- [57] Y. Zhou, C. Huang, Q. Liao, and P. Lu, *Phys. Rev. Lett.* **109**, 053004 (2012).
- [58] Y. Zhou, Q. Zhang, C. Huang, and P. Lu, *Phys. Rev. A* **86**, 043427 (2012).
- [59] A. Tong, Y. Zhou, and P. Lu, *Opt. Express* **23**, 15774 (2015).
- [60] E. Lötstedt, T. Kato, and K. Yamanouchi, *Phys. Rev. Lett.* **106**, 203001 (2011).
- [61] A. E. S. Green, D. L. Sellin, and A. S. Zachor, *Phys. Rev.* **184**, 1 (1969).
- [62] X. M. Tong, Z. X. Zhao, and C. D. Lin, *Phys. Rev. A* **66**, 033402 (2002).
- [63] C. O. Reinhold and R. E. Olson, *Phys. Rev. A* **39**, 3861 (1989).
- [64] L. D. Landau and E. M. Lifshitz, *Quantum Mechanics* (Pergamon, Oxford, 1977).
- [65] B. Hu, J. Liu, and S. G. Chen, *Phys. Lett. A* **236**, 533 (1997).
- [66] L. B. Fu, J. Liu, J. Chen, and S. G. Chen, *Phys. Rev. A* **63**, 043416 (2001).
- [67] H. Price, C. Lazarou, and A. Emmanouilidou, *Phys. Rev. A* **90**, 053419 (2014).
- [68] N. B. Delone and V. P. Krainov, *J. Opt. Soc. Am. B* **8**, 1207 (1991).
- [69] P. Kustaanheimo and E. Stiefel, *J. Reine Angew. Math.* **218**, 204 (1965).